IFITM3 protects the heart during influenza virus infection

Adam D. Kenney[a,b], Temet M. McMichael[a], Alexander Imas[a], Nicholas M. Chesarino[a], Lizhi Zhang[a,b], Lisa E. Dorn[c], Qian Wu[a], Omar Alfaour[a], Foued Amari[d], Min Chen[d], Ashley Zani[a,b], Mahesh Chemudupati[a,b], Federica Accornero[b,c], Vincenzo Coppola[b,d,e], Murugesan V. S. Rajaram[a,b,1], and Jacob S. Yount[a,b,1]

[a]Department of Microbial Infection and Immunity, The Ohio State University, Columbus, OH 43210; [b]Infectious Diseases Institute, The Ohio State University, Columbus, OH 43210; [c]Department of Physiology and Cell Biology, The Ohio State University, Columbus, OH 43210; [d]Genetically Engineered Mouse Modeling Core, The Ohio State University and James Comprehensive Cancer Center, Columbus, OH 43210; and [e]Department of Cancer Biology and Genetics, The Ohio State University, Columbus, OH 43210

Influenza virus can disseminate from the lungs to the heart in severe infections and can induce cardiac pathology, but this has been difficult to study due to a lack of small animal models. In humans, polymorphisms in the gene encoding the antiviral restriction factor IFN-induced transmembrane protein 3 (IFITM3) are associated with susceptibility to severe influenza, but whether IFITM3 deficiencies contribute to cardiac dysfunction during infection is unclear. We show that IFITM3 deficiency in a new knockout (KO) mouse model increases weight loss and mortality following influenza virus infections. We investigated this enhanced pathogenesis with the A/PR/8/34 (H1N1) (PR8) influenza virus strain, which is lethal in KO mice even at low doses, and observed increased replication of virus in the lungs, spleens, and hearts of KO mice compared with wild-type (WT) mice. Infected IFITM3 KO mice developed aberrant cardiac electrical activity, including decreased heart rate and irregular, arrhythmic RR (interbeat) intervals, whereas WT mice exhibited a mild decrease in heart rate without irregular RR intervals. Cardiac electrical dysfunction in PR8-infected KO mice was accompanied by increased activation of fibrotic pathways and fibrotic lesions in the heart. Infection with a sublethal dose of a less virulent influenza virus strain (A/WSN/33 [H1N1]) resulted in a milder cardiac electrical dysfunction in KO mice that subsided as the mice recovered. Our findings reveal an essential role for IFITM3 in limiting influenza virus replication and pathogenesis in heart tissue and establish IFITM3 KO mice as a powerful model for studying mild and severe influenza virus-induced cardiac dysfunction.

influenza | interferon | IFITM3 | heart

Influenza virus is among the top 10 causes of human mortality and costs the US economy as much as $80 billion per year due to lost productivity (1). Although influenza virus primarily infects the lungs, cardiac complications of infection are also well documented (2–8). Influenza virus is known to be a cardiotropic virus that can disseminate from the lungs to infect heart tissue, particularly during severe infections (9–12). Thus, the virus can cause myocarditis and cardiac dysfunction even in individuals without preexisting cardiovascular disease. Signs of myocarditis have been observed in up to 13% of individuals hospitalized with influenza virus infections (2–4). Furthermore, myocarditis has been reported at autopsy in up to 48% of fatal seasonal influenza cases (4–7), and a landmark autopsy study reported severe cardiac damage in a majority of 126 patients examined after succumbing to infection with the 1918 pandemic H1N1 influenza virus (8). Infections of cynomolgus macaques with the 1918 virus showed that the virus disseminated to the heart as early as 3 d postinfection (11). But although severe influenza virus infections are associated with heart infection and pathology, the underlying mechanisms of and susceptibility factors for these effects are poorly understood.

Influenza A virus (IAV) infections of extrapulmonary tissues, including the heart, spleen, kidney, thymus, and brain, have been reported for various mouse models of infection (9, 10, 13). However, relevant models in which significant cardiac pathogenesis

occurs are lacking, hindering advancement in the study of cardiac complications of influenza virus infection. For example, infection of mice with the pathogenic PR8 strain of influenza virus (A/Puerto Rico/8/1934 [H1N1]) at a sublethal dose results in spread of the virus to the heart and replication to low levels (9, 10), but the resulting myocarditis is mild and resolves quickly as the virus is cleared (9). Infections with extreme virus doses can cause increased pathogenesis and lethality, but the rapid death induced by such infection regimens might not involve the same pathogenic mechanisms as are initiated during a longer course of infection with a lower dose (14, 15). Likewise, animals lacking the type I IFN receptor or downstream signaling molecules experience increased pathogenicity on infection (16, 17), but deficiencies in these animals correspond to genetic defects that are rarely seen in humans (18). Thus, there is a need for an animal model displaying significant cardiac complications of influenza virus infection in which the animal's susceptibility is relevant to human infections and in which a physiologically relevant virus dose is administered via the intranasal route.

Single nucleotide polymorphisms (SNPs) in the *IFITM3* gene or its promoter are among the only genetic defects that have been reproducibly associated with severe influenza in humans (18–24). IFITM3 directly restricts influenza virus infection by inhibiting virus entry into cells, and it also provides a secondary function in dampening tissue-damaging inflammatory cytokine responses (25–30). The rs12252-C SNP has been suggested to cause IFITM3 mislocalization and thus an inability to inhibit influenza virus infections (19, 31). In the Han Chinese

---

Significance

We discovered that IFITM3 prevents efficient dissemination and replication of influenza virus in heart tissue, thereby limiting cardiac fibrosis and electrical dysfunction during infection. Since IFITM3 polymorphisms are among the only human genetic factors that have been reproducibly associated with hospitalization and mortality during influenza virus infection, our findings are relevant to the serious threat of influenza virus infection to human health. Furthermore, IFITM3 KO mice provide one of the first models for studying cardiac complications of influenza.

population, this SNP is homozygous in 20% of individuals (23). Another SNP, rs34481144-A, located in the IFITM3 promoter, is homozygous in 4% of people with European ancestry (23). These individuals produce low levels of IFITM3, making them more susceptible to infection (22). Given that numerous studies have linked IFITM3 defects to severe influenza virus infections, and that severe influenza virus infections may include cardiac complications, we sought to investigate whether IFITM3 plays a role in protecting the heart during infection.

Results

Generation of the IFITM3 KO Mouse Model. IFITM3 KO mice used in previous infection research are of a mixed genetic background and contain a fluorescent protein insertion at the IFITM3 locus (32). To generate a mouse model with a clean genetic deficiency on a pure C57BL/6 background, we used a CRISPR/Cas9-based deletion strategy involving 2 guide RNAs with unique sequence identity for a region of exon 1 of the *Ifitm3* gene (Fig. 1*A*). Mutant pups with an *Ifitm3* deletion were identified by PCR (Fig. 1*B*). In 1 targeted animal, sequencing confirmed deletion of a 53-bp region of exon 1. As a specificity control, RT-PCR for full-length IFITM1, IFITM2, and IFITM3 coding sequences was performed on mRNA from WT and mutant (termed IFITM3 KO) mouse embryonic fibroblasts (MEFs). The resulting PCR products showed a band shift in the KO cells for IFITM3 only (Fig. 1*C*), and DNA sequencing of the PCR products confirmed that IFITM1 and IFITM2 sequences were not mutated. Despite low probability scores, we DNA-sequenced the top 5 off-target sites for each guide RNA as predicted by Benchling software and did not observe any mutations (*SI Appendix*, Fig. S1). The *Ifitm3* deletion introduces a nonsense mutation at codon 18 and a subsequent stop codon at position 37 (Fig. 1*A*). Importantly, motifs essential for IFITM3 antiviral activity, membrane association, localization, and dimerization are not contained within its N-terminal

17 amino acids (23, 27, 31, 33, 34). IFITM3 protein could not be detected by immunoblotting of tissue or cell lysates derived from the KO mice, even on IFNβ treatment (Fig. 1 *D* and *E*).

Given the well-characterized role of IFITM3 in blocking influenza virus infection of cells (35, 36), we examined the susceptibility of MEFs derived from WT and KO mice to infection with H1N1 IAV virus (PR8 strain). KO cells were significantly more susceptible to infection than WT cells even after IFN treatment, which caused decreased susceptibility to infection in WT cells (Fig. 1*F* and *SI Appendix*, Fig. S2). We observed similar trends on influenza virus infection of WT and IFITM3 KO bone marrow-derived macrophages (*SI Appendix*, Fig. S3). These results confirm previous experiments from our group and others indicating that IFITM3 is responsible for a significant portion of the anti-influenza response induced by type I IFN (35, 37, 38).

We next examined vesicular stomatitis virus (VSV) infection of WT and KO MEFs. VSV is highly susceptible to inhibition by IFN, and although it is reported to be mildly inhibited when IFITM3 is highly overexpressed, VSV has not been tested for susceptibility to inhibition by endogenous levels of mouse IFITM3 (39). Unlike influenza virus infections, WT and KO cells were infected at similar rates by VSV, and VSV infection was fully restricted by IFN treatment regardless of IFITM3 status (Fig. 1*F* and *SI Appendix*, Fig. S2). These results indicate that endogenous baseline IFITM3 does not inhibit VSV infection, and that IFITM3 is not a significant contributor to the type I IFN-induced inhibition of VSV in MEFs.

These infection experiments provide important controls demonstrating that cells derived from IFITM3 KO animals are not indiscriminately susceptible to all viruses, and that the antiviral IFN response is otherwise functional in IFITM3 KO cells.

Increased Morbidity and Mortality of IFITM3 KO Mice on Influenza A Virus Infection. To examine the pathogenesis of IAV infection in IFITM3 KO versus WT mice, we infected mice intranasally with
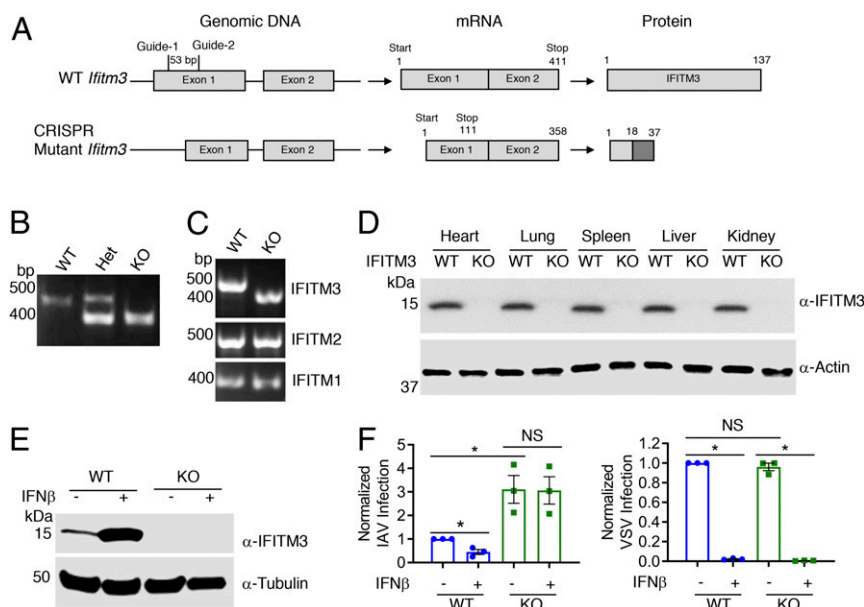

Fig. 1. Generation and validation of our IFITM3 KO C57BL/6 mouse model. (*A*) C57BL/6 zygotes were injected with a mix of Cas9 mRNA and 2 guide RNAs to target exon 1 of the *Ifitm3* gene. As a result of a 53-bp deletion and consequent frame shift, the mutant Δ53 IFITM3 KO gene bears a nonsense mutation at codon 18 and a subsequent stop codon at position 37. The protein depicted for the mutant is hypothetical. (*B*) Example genotyping PCR on genomic DNA from WT, heterozygous (het), and KO mice. Sequencing of the PCR products revealed a 53-bp deletion in the KO allele. (*C*) RT-PCR for IFITM1, IFITM2, and IFITM3 performed on mRNA extracted from IFNβ-treated MEFs obtained from mice of the indicated genotypes. Sequencing of the PCR products confirmed the 53-bp deletion in the IFITM3 mRNA in IFITM3 KO cells and no mutation of IFITM1 and IFITM2 sequences. (*D*) Western blot analysis of tissue lysates from WT and IFITM3 KO mice. (*E*) MEFs derived from embryos of the indicated genotypes were treated with IFNβ or mock-treated, and lysates were subjected to Western blot analysis. (*F*) MEFs treated as in *E* were infected with IAV or VSV for 24 h, and percent infection was determined by flow cytometry. Graphs depict normalized measurements from at least 3 separate experiments. Relevant comparisons were analyzed by unpaired *t* tests as indicated by lines. *$P < 0.001$. NS, not significant.

the PR8 strain at a dose of 10 $TCID_{50}$, the lowest dose that allowed reproducible infections in our experiments. This dose caused weight loss in WT mice, but the mice began to recover by day 12 postinfection (Fig. 2A). KO mice lost significantly more weight starting at day 4 postinfection and continuing throughout the remainder of infection (Fig. 2A). By day 12 postinfection, all KO mice had succumbed to infection or had lost more than 30% of their body weight and were euthanized (Fig. 2B). Virus titers in the lungs measured on days 5, 7, and 10 postinfection were found to be higher in KO versus WT mice at each time point (Fig. 2C). Relative to earlier time points in WT mice, day 10 virus titers were decreased, indicating adaptive immune clearance of the virus (Fig. 2C). In contrast, titers in the IFITM3 KO lungs on day 10 remained high (Fig. 2C). We also examined levels of the representative inflammatory cytokine IL-6 in lung homogenates at these postinfection time points and found higher levels of IL-6 in the KO lungs compared with WT lungs at all time points (Fig. 2D). Overall, relative to WT mice, IFITM3 KO mice were more severely infected by influenza virus strain PR8.

Influenza Virus Replicates to High Levels in the Heart in the Absence of IFITM3. We next investigated whether in addition to the lung, virus disseminated to higher levels in other organs of IFITM3 KO mice, including the heart. We quantified virus titers in the hearts of infected animals on days 5, 7, and 10 postinfection. We observed a modest increase in virus titers in the hearts of KO mice compared with WT mice on day 5 postinfection, followed by markedly higher titers on days 7 and 10 (Fig. 3A). As seen in the lung, on day 10 postinfection, the virus titers remained high in hearts of KO mice but had declined substantially in WT mice (Figs. 2C and 3A). In fact, in WT mice, the low virus levels in the heart on days 5 and 7 were cleared to below the limit of detection by day 10, but remained at a titer similar to that seen on day 7 in KO mice (Fig. 3A).

To examine whether cells in the heart were directly infected with influenza virus, we stained heart sections from WT and KO mice on day 10 postinfection with anti-influenza virus nucleoprotein antibody. We observed minimal staining of the WT

hearts, but found staining of elongated cells consistent with a cardiac fibroblast morphology and localization in KO hearts (Fig. 3B). We next costained heart sections for virus antigen and vimentin, a marker of cardiac fibroblasts, and found that virus infection in KO hearts was particularly apparent in enlarged vimentin-positive cells (SI Appendix, Fig. S4). Interestingly, in WT hearts, IFITM3 is highly expressed in vimentin-positive cardiac fibroblasts (SI Appendix, Fig. S5A). Unexpectedly, we observed a small decrease in the number of cardiac fibroblasts in 4 out of 6 KO hearts at day 10 postinfection (SI Appendix, Fig. S5B). This modest depletion may be due to direct infection of the fibroblasts, which could promote cell death.

The high level of virus in the lungs and hearts of KO animals prompted us to examine whether virus disseminated to other organs. We observed a significant increase in spleen viral titer in the KO mice at day 10 postinfection compared with WT, but detected no virus in the liver, kidney, or brain of either WT or KO mice (Fig. 3C). The differences between WT and KO mice show that virus replication is inadequately controlled in each of the IFITM3 KO organs in which we detected influenza virus, including the heart.

Influenza Virus Infection Causes Cardiac Electrical Dysfunction in IFITM3 KO Mice. Given that replication of influenza virus to high titers in the heart has been seen only rarely in mouse models (9, 10), we sought to examine the effect of the high virus loads in the hearts of IFITM3 KO mice on cardiac electrical function. First, we determined that IFITM3 KO mice exhibit cardiac function and activity at baseline comparable to that seen in WT mice as measured by both echocardiography and electrocardiography (ECG) (SI Appendix, Fig. S6). Next, we performed ECG measurements on WT and KO mice after infection with PR8 as previously established (Fig. 2). Both WT and KO mice showed depressed heart rates and increased RR interval (i.e., the interbeat time interval between the major R peaks of the ECG traces) averages at day 6 postinfection (Fig. 4A). WT mice returned to a normal heart rate and average RR interval duration by day 10, while the electrical activity of the KO mice continued to decline significantly (Fig. 4A). Importantly, these differing cardiac measurements correlate with high virus titers detected in the KO hearts and with virus clearance in the WT hearts (Fig. 3A).

In addition to higher average RR interval values in the infected KO mice, we observed highly irregular RR intervals late in infection in KO mice with no discernible pattern, while RR intervals in WT mice remained regularly paced, comparable to those seen in mock-infected animals (Fig. 4B). Plotting of individual RR interval times revealed a higher level of variability in KO mice compared with WT mice (Fig. 4C). Indeed, RR interval ranges calculated for 5-min ECG readings in multiple mice confirmed a significant arrhythmia that was consistently observed in KO mice (Fig. 4D).

We next performed infections with 2 less pathogenic strains of IAV compared with PR8 to examine whether these strains could also cause cardiac electrical dysfunction. These included X31, a PR8 reassortant virus containing the HA and NA segments from A/Hong Kong/1/1968 (H3N2) and A/WSN/1933 (H1N1) known as WSN. We chose a dose of X31, 1,000 $TCID_{50}$, that caused measurable weight loss in WT mice (SI Appendix, Fig. S7A). This dose resulted in a greater decline in weight in KO mice and delayed recovery (SI Appendix, Fig. S7A). However, infection with this less pathogenic strain did not result in significant cardiac electrical changes (SI Appendix, Fig. S7 B and C), and thus we did not investigate X31 further. For WSN infections, we used a dose of 200 $TCID_{50}$, which caused weight loss in WT mice and was more virulent in KO mice, but did not cause lethality (SI Appendix, Fig. S8A). WSN infection caused moderate electrical dysfunction, including decreased heart rate and irregular RR intervals, by day 8 postinfection that abated by day 10 postinfection
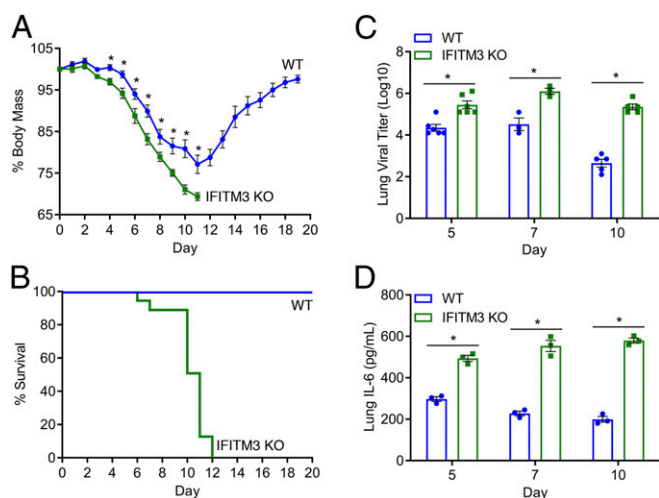

Fig. 2. IFITM3 KO mice experience increased morbidity and mortality on influenza virus infection. (A and B) WT (n = 29) and IFITM3 KO (n = 21) mice were intranasally infected with IAV strain PR8 (10 $TCID_{50}$) and followed daily for weight loss (A) and survival (B). Points in A depict mean values, and error bars represent SD of the mean. *P < 0.01, unpaired t test. (C) Infected mice were killed on the indicated days for $TCID_{50}$ measurement of virus titers in the lung. Data points collected for days 5 and 10 were from 2 independent experiments. (D) ELISA quantification of IL-6 in lungs collected on the indicated days postinfection. In C and D, each point represents an individual mouse, and bars represent mean values. Error bars represent SD of the mean. *P < 0.001, unpaired t test.
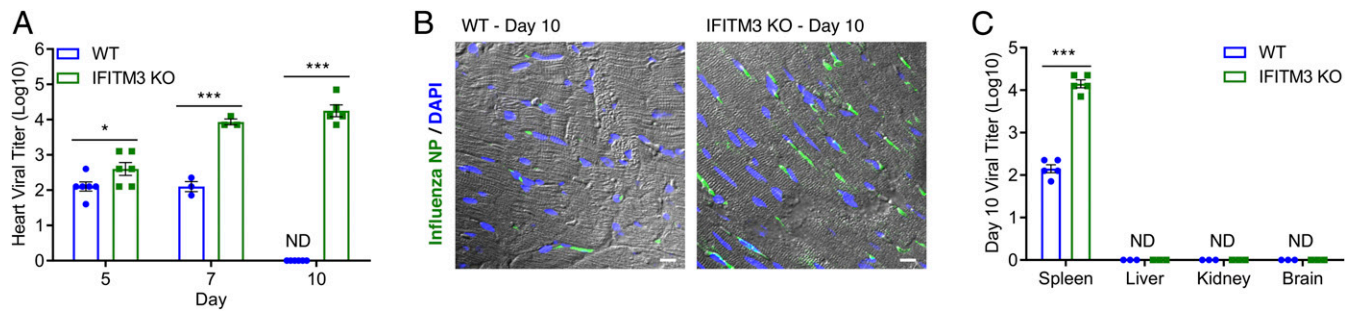
Fig. 3. IFITM3 KO mice show uncontrolled influenza virus replication in the heart. WT and IFITM3 KO mice were intranasally infected with IAV strain PR8 (10 $TCID_{50}$). (A) Infected mice were killed on day 5, 7, or 10 postinfection for $TCID_{50}$ measurement of virus titers in the heart. Data points collected for days 5 and 10 were from 2 independent experiments. Each point represents an individual mouse, and bars represent mean values. Error bars represent SD of the mean. *$P < 0.05$, ***$P < 0.0001$, unpaired t test. ND, not detected. (B) Representative images of heart sections from mice killed on day 10 postinfection. Green, anti-influenza virus nucleoprotein (NP) staining; blue, DAPI; gray, brightfield imaging. (Scale bar: 10 μm.) (C) Infected mice were killed on day 10 postinfection for $TCID_{50}$ measurement of virus titers in the spleen, liver, kidney, and brain. Each point represents an individual mouse, and bars represent mean values. Error bars represent SD of the mean. ***$P < 0.0001$, unpaired t test. ND, not detected.

as the mice began to recover (*SI Appendix*, Fig. S8 B–E). These WSN infection data, along with data from WT mice infected with PR8 (Fig. 4A and *SI Appendix*, Fig. S8B), indicate that mild or moderate cardiac dysfunction during influenza virus infection is reversible. Furthermore, these results show that the inherent virulence of individual virus strains, along with the increased susceptibility caused by IFITM3 KO, determine the severity of cardiac dysfunction during influenza virus infection.

IFITM3 Protects Mice from Excess Collagen Deposition in the Heart during Infection. Cardiac fibrosis results from excess fibroblast secretion of extracellular matrix components, particularly collagen, and unresolved collagen accumulation has been shown to

reduce the efficiency of electrical conductivity of the heart (40, 41). Thus, we hypothesized that fibrotic collagen deposition may be linked to the severe cardiac electrical defects observed in PR8-infected IFITM3 KO mice. We examined heart sections from PR8-infected WT and KO mice at day 10 postinfection after Masson's trichrome staining, which allows visualization of collagen via blue staining. We observed significantly more blue staining in the hearts of KO animals, indicating an increased fibrotic response (Fig. 5 A and B). Importantly, we did not observe baseline fibrosis in mock-infected WT or IFITM3 KO hearts (Fig. 5 A and B). Given that we observed direct infection and depletion of cardiac fibroblasts in infected IFITM3 KO mice (*SI Appendix*, Figs. S4 and S5), this fibrotic response cannot be explained by an increase in
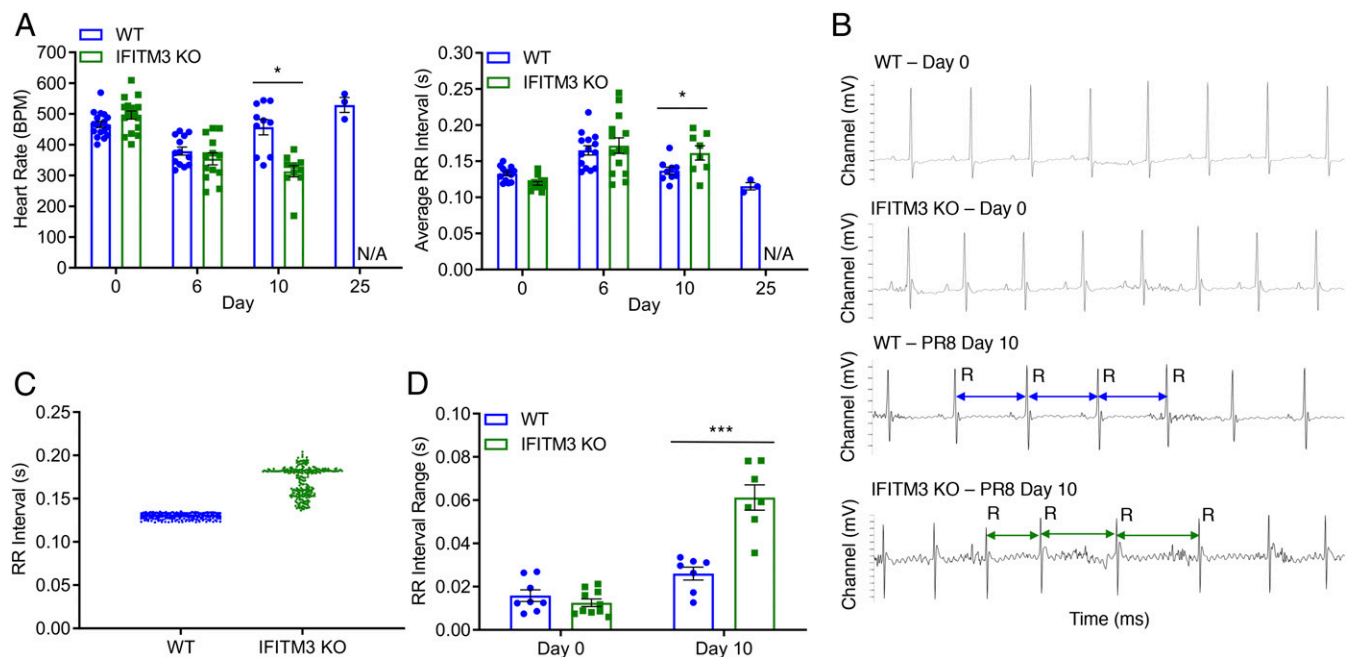

Fig. 4. IFITM3 KO mice suffer from cardiac electrical dysfunction following influenza virus infection. WT and IFITM3 KO mice were intranasally infected with IAV strain PR8 (10 $TCID_{50}$). (A) ECG measurements over the time course of infection. Except for day 25, data were collected over at least 3 independent experiments. Each point represents an individual mouse, and bars represent mean values. Error bars represent SD of the mean. *$P < 0.05$, unpaired t test. (B) Example ECG readings from WT and KO mice preinfection and postinfection with PR8. Selected RR intervals of the infected mice are highlighted by blue (WT) or green (KO) double arrows. (C) RR interval times plotted for a representative WT mouse and a representative IFITM3 KO mouse on day 10 postinfection. (D) RR ranges, defined as the difference between the longest and shortest RR intervals over an ECG measurement period of 5 min, were calculated for individual mice on day 10 postinfection. Each point represents an individual mouse, and bars represent mean values. Error bars represent SD of the mean. ***$P < 0.0001$, unpaired t test.

fibroblast numbers, suggesting that activation, rather than overall numbers of fibroblasts, may underlie this phenotype.

We also confirmed via qRT-PCR analysis that collagen gene (Col1A2) expression was increased in infected KO hearts at day 10 postinfection (Fig. 5C). Since collagen up-regulation is often associated with induction by TGFβ signaling, we also examined Tgfb1 gene expression in the hearts of infected animals and found that it was also up-regulated in KO hearts compared with WT hearts (Fig. 5D). In addition, we measured IL-6 levels in heart tissue after infection, because we observed infection of cardiac cells via microscopy analysis (Fig. 3B), and IL-6 is induced directly by influenza virus infection via activation of the RIG-I signaling pathway (42), and because IL-6 is associated

with cardiac fibrosis via TGFβ induction in cardiac fibroblasts (43). We detected significantly higher amounts of IL-6 protein as measured by enzyme-linked immunosorbent assay (ELISA) in heart homogenates from infected KO mice compared with WT mice (Fig. 5E). In sum, these data show that fibrotic pathways are activated at higher levels in the hearts of infected KO mice, resulting in excess collagen deposition. These experiments showing an enhanced fibrotic response further highlight the critical cardiac protection afforded by IFITM3 during IAV infection, thus identifying a new essential role for this innate immunity protein.

Discussion

There is an underappreciated, but well-documented, effect of severe influenza virus infections in causing cardiac pathologies even in individuals without underlying cardiovascular disease (2–8, 44, 45). Whether these effects are caused by systemic inflammation or direct infection of heart tissue remains an area of debate, although virus has been detected in human heart samples (46–49). Given that genetic defects in IFITM3 are associated with severe influenza in humans (18–24), we investigated whether cardiac complications of influenza virus infection occur in an IFITM3 KO mouse model. We discovered that IFITM3 limits levels of virus in the heart during PR8 infection (Fig. 3). We observed that high virus loads in the hearts of IFITM3 KO mice are accompanied by increased activation of fibrotic pathways and cardiac electrical dysfunction (Figs. 4 and 5). Thus, in addition to identifying a novel function for IFITM3 in protecting the heart, we have also established IFITM3 KO mice as a model system for the study of cardiac complications of influenza virus infections. This mouse model provides an unprecedented opportunity to study the molecular mechanisms underlying cardiac pathology induced during influenza virus infection.

We observed varying levels of morbidity and cardiac dysfunction during infections with specific strains of IAV. Distinct from the PR8 (H1N1) strain, we found that both WSN (H1N1) and X31 (H3N2) caused increased weight loss, but not lethality, in the IFITM3 KO mice (Fig. 2 A and B and SI Appendix, Figs. S7 and S8). WSN infection caused moderate cardiac electrical dysfunction that subsided as the mice recovered (SI Appendix, Fig. S8), whereas X31 infection caused no discernable cardiac changes (SI Appendix, Fig. S7). This is particularly interesting because X31 is a reassortant virus differing from PR8 in only its HA (H3) and NA (N2) genomic segments, suggesting that the cardiac effects of IAV infection are influenced by the identity of the viral surface glycoproteins. Overall, we have identified model viruses for which infections of IFITM3 KO animals result in a spectrum of cardiac phenotypes: X31 (no cardiac phenotype), WSN (moderate electrical defects that subside), and PR8 (severe electrical defects before lethality).

Cardiac complications of infection are likely determined by a combination of host susceptibility and viral pathogenicity. Human IFITM3 polymorphisms have been linked to hospitalization or death during infection with various IAV strains in numerous studies (18–24). Drawing parallels to our mouse experiments in which IFITM3 KO mice develop severe infections (Figs. 2 and 4), including cardiac dysfunction, we speculate that individuals with IFITM3 defects may be more susceptible to influenza virus replication in the heart. It is interesting to note that not all influenza virus strains cause the same cardiac phenotype in IFITM3 KO mice, which is likely the case in human infections as well. Identification of WSN as a strain that causes moderate and reversible cardiac electrical defects in IFITM3 KO mice suggests that this model may eventually allow the study of repeated cardiac insults.

Questions remain regarding the cardiac pathogenesis of influenza virus infection. For example, molecular pathways activated by cardiac infection that lead to cardiac dysfunction remain to be fully elucidated and may involve up-regulation of cytokines, such as IL-6 and TGFβ, as well as collagen downstream of these
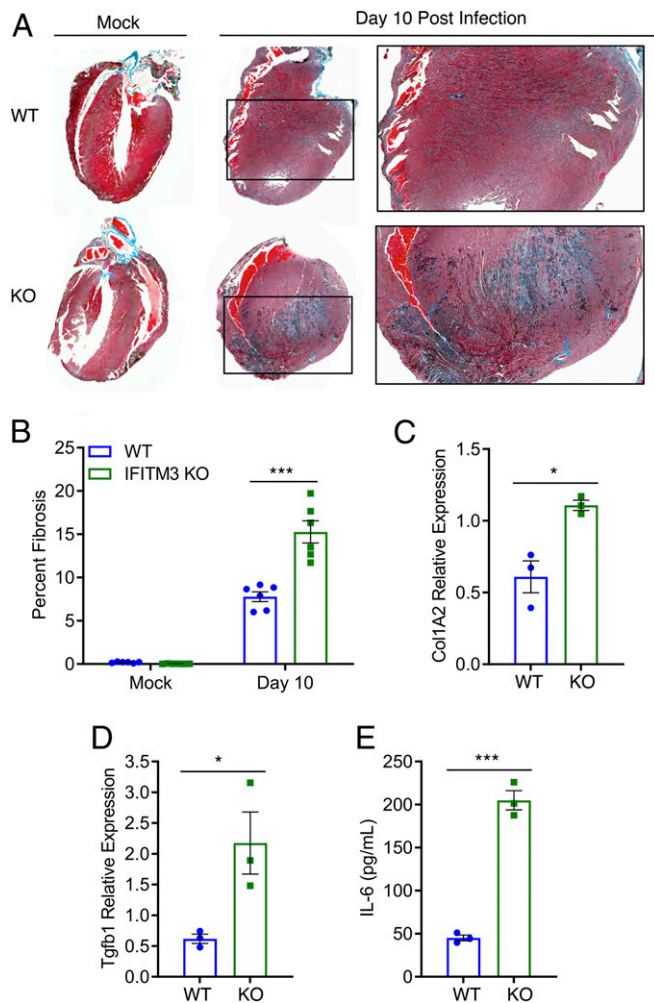
Fig. 5. Cardiac fibrosis in influenza virus infection of IFITM3 KO mice. WT and IFITM3 KO mice were intranasally infected with influenza virus strain PR8 (10 $TCID_{50}$) or were mock-infected. (A) Hearts were collected on day 10 postinfection, and sections were stained with Masson's trichrome stain, in which blue staining is indicative of fibrotic collagen deposition. A representative infected heart and a representative mock-infected sample are shown for each genotype. Boxed areas are regions magnified in the far-right images. (B) Blue pixel percentages from images as in A were quantified for mock-infected and infected WT and KO hearts using ImageJ software. (C and D) qRT-PCR on mRNA extracted from hearts collected at day 10 postinfection was performed to assess expression of Col1A2 (C) and Tgfb1 (D). (E) IL-6 ELISA was performed on heart homogenates collected on day 10 postinfection. In B–E, each point represents a heart from an individual mouse, and bars represent mean values. Error bars represent SD of the mean. *$P < 0.05$, ***$P < 0.0001$, unpaired t test.

cytokines. Similarly, the role of immune cells in cardiac dysfunction caused by influenza virus infection is unknown. In this regard, it is not clear why virus levels in the lungs, spleen, and heart are not controlled by the adaptive immune system in IFITM3 KO mice (Figs. 2C and 3 A and C), although this may be explained by previous studies showing that some T cell populations are protected from direct infection and death by their expression of IFITM3 (22, 50). Interestingly, our data on less pathogenic influenza virus strains demonstrate that IFITM3 KO mice are capable of recovery after sublethal infections (SI Appendix, Figs. S7 and S8), which generally indicates that the adaptive immune response is functional in clearing the virus. Overall, our newly generated IFITM3 KO mice and distinct models of IAV virulence provide powerful tools for probing these intriguing questions in future experiments.

Materials and Methods

IFITM3 KO mice were generated by CRISPR/Cas9 technology at the Genetically Engineered Mouse Modeling Core of The Ohio State University. Here 6- to 10-wk-old mice were anesthetized with isoflurane and intranasally infected with IAV strain PR8 (10 $TCID_{50}$), IAV strain WSN (200 $TCID_{50}$), or IAV strain ×31 (1,000 $TCID_{50}$) in sterile saline, or were mock-infected with saline in some experiments. ECG recordings were performed on anesthetized mice using the lead II configuration with s.c. electrodes for 3 to 5 min per mouse. Organs collected from euthanized mice at indicated time points were fixed in formalin and sectioned for histology or were homogenized in PBS for calculation of virus titer/cytokine levels. Detailed descriptions of the methodologies are provided in SI Appendix.

1. N. A. Molinari et al., The annual impact of seasonal influenza in the US: Measuring disease burden and costs. Vaccine 25, 5086–5096 (2007).
2. M. Kodama, Influenza myocarditis. Circ. J. 74, 2060–2061 (2010).
3. J. Karjalainen, M. S. Nieminen, J. Heikkilä, Influenza A1 myocarditis in conscripts. Acta Med. Scand. 207, 27–30 (1980).
4. A. Ukimura, Y. Ooi, Y. Kanzaki, T. Inomata, T. Izumi, A national survey on myocarditis associated with influenza H1N1pdm2009 in the pandemic and postpandemic season in Japan. J. Infect. Chemother. 19, 426–431 (2013).
5. R. Oseasohn, L. Adelson, M. Kaji, Clinicopathologic study of thirty-three fatal cases of Asian influenza. N. Engl. J. Med. 260, 509–518 (1959).
6. C. D. Paddock et al., Myocardial injury and bacterial pneumonia contribute to the pathogenesis of fatal influenza B virus infection. J. Infect. Dis. 205, 895–905 (2012).
7. A. Ukimura, T. Izumi, A. Matsumori; Clinical Research Committee on Myocarditis Associated with 2009 Influenza A (H1N1) Pandemic in Japan organized by Japanese Circulation Society, A national survey on myocarditis associated with the 2009 influenza A (H1N1) pandemic in Japan. Circ. J. 74, 2193–2199 (2010).
8. B. Lucke, T. Wight, E. Kime, Pathologic anatomy and bacteriology of influenza: Epidemic of autumn, 1918. Arch. Intern. Med. 24, 154–237 (1919).
9. M. Kotaka, Y. Kitaura, H. Deguchi, K. Kawamura, Experimental influenza A virus myocarditis in mice: Light and electron microscopic, virologic, and hemodynamic study. Am. J. Pathol. 136, 409–419 (1990).
10. T. Fislová et al., Multiorgan distribution of human influenza A virus strains observed in a mouse model. Arch. Virol. 154, 409–419 (2009).
11. D. Kobasa et al., Aberrant innate immune response in lethal infection of macaques with the 1918 influenza virus. Nature 445, 319–323 (2007).
12. K. Iwatsuki-Horimoto et al., The marmoset as an animal model of influenza: Infection with A(H1N1)pdm09 and highly pathogenic A(H5N1) viruses via the conventional or tracheal spray route. Front. Microbiol. 9, 844 (2018).
13. S. Tundup et al., Endothelial cell tropism is a determinant of H5N1 pathogenesis in mammalian species. PLoS Pathog. 13, e1006270 (2017).
14. P. S. Woods et al., Lethal H1N1 influenza A virus infection alters the murine alveolar type II cell surfactant lipidome. Am. J. Physiol. Lung Cell. Mol. Physiol. 311, L1160–L1169 (2016).
15. A. J. Vogel, S. Harris, N. Marsteller, S. A. Condon, D. M. Brown, Early cytokine dysregulation and viral replication are associated with mortality during lethal influenza infection. Viral Immunol. 27, 214–224 (2014).
16. A. García-Sastre et al., The role of interferon in influenza virus tissue tropism. J. Virol. 72, 8550–8558 (1998).
17. K. J. Szretter et al., Early control of H5N1 influenza virus replication by the type I interferon response in mice. J. Virol. 83, 5825–5834 (2009).
18. A. D. Kenney et al., Human genetic determinants of viral diseases. Annu. Rev. Genet. 51, 241–263 (2017).
19. A. R. Everitt et al.; GenISIS Investigators; MOSAIC Investigators, IFITM3 restricts the morbidity and mortality associated with influenza. Nature 484, 519–523 (2012).
20. Y. Pan et al., IFITM3 Rs12252-C variant increases potential risk for severe influenza virus infection in Chinese population. Front. Cell. Infect. Microbiol. 7, 294 (2017).
21. Z. Wang et al., Early hypercytokinemia is associated with interferon-induced transmembrane protein-3 dysfunction and predictive of fatal H7N9 infection. Proc. Natl. Acad. Sci. U.S.A. 111, 769–774 (2014).
22. E. K. Allen et al., SNP-mediated disruption of CTCF binding at the IFITM3 promoter is associated with risk of severe influenza in humans. Nat. Med. 23, 975–983 (2017).
23. A. Zani, J. S. Yount, Antiviral protection by IFITM3 in vivo. Curr. Clin. Microbiol. Rep. 5, 229–237 (2018).
24. Y. H. Zhang et al., Interferon-induced transmembrane protein-3 genetic variant rs12252-C is associated with severe influenza in Chinese individuals. Nat. Commun. 4, 1418 (2013).
25. T. M. Desai et al., IFITM3 restricts influenza A virus entry by blocking the formation of fusion pores following virus-endosome hemifusion. PLoS Pathog. 10, e1004048 (2014).
26. E. M. Feeley et al., IFITM3 inhibits influenza A virus infection by preventing cytosolic entry. PLoS Pathog. 7, e1002337 (2011).
27. N. M. Chesarino et al., IFITM3 requires an amphipathic helix for antiviral activity. EMBO Rep. 18, 1740–1751 (2017).
28. K. Li et al., IFITM proteins restrict viral membrane hemifusion. PLoS Pathog. 9, e1003124 (2013).
29. M. A. Stacey et al., The antiviral restriction factor IFN-induced transmembrane protein 3 prevents cytokine-driven CMV pathogenesis. J. Clin. Invest. 127, 1463–1474 (2017).
30. L. Q. Jiang et al., IFITM3 inhibits virus-triggered induction of type I interferon by mediating autophagosome-dependent degradation of IRF3. Cell. Mol. Immunol. 15, 858–867 (2018).
31. N. M. Chesarino, T. M. McMichael, J. C. Hach, J. S. Yount, Phosphorylation of the antiviral protein interferon-inducible transmembrane protein 3 (IFITM3) dually regulates its endocytosis and ubiquitination. J. Biol. Chem. 289, 11986–11992 (2014).
32. U. C. Lange et al., Normal germ line establishment in mice carrying a deletion of the Ifitm/Fragilis gene family cluster. Mol. Cell. Biol. 28, 4688–4696 (2008).
33. J. S. Yount, R. A. Karssemeijer, H. C. Hang, S-palmitoylation and ubiquitination differentially regulate interferon-induced transmembrane protein 3 (IFITM3)-mediated resistance to influenza virus. J. Biol. Chem. 287, 19631–19641 (2012).
34. N. M. Chesarino, T. M. McMichael, J. S. Yount, E3 ubiquitin ligase NEDD4 promotes influenza virus infection by decreasing levels of the antiviral protein IFITM3. PLoS Pathog. 11, e1005095 (2015).
35. A. L. Brass et al., The IFITM proteins mediate cellular resistance to influenza A H1N1 virus, West Nile virus, and dengue virus. Cell 139, 1243–1254 (2009).
36. J. S. Yount et al., Palmitoylome profiling reveals S-palmitoylation-dependent antiviral activity of IFITM3. Nat. Chem. Biol. 6, 610–614 (2010).
37. T. Y. Lin et al., Amphotericin B increases influenza A virus infection by preventing IFITM3-mediated restriction. Cell Rep. 5, 895–908 (2013).
38. T. M. McMichael et al., The palmitoyltransferase ZDHHC20 enhances interferon-induced transmembrane protein 3 (IFITM3) palmitoylation and antiviral activity. J. Biol. Chem. 292, 21517–21526 (2017).
39. J. M. Weidner et al., Interferon-induced cell membrane proteins, IFITM3 and tetherin, inhibit vesicular stomatitis virus infection via distinct mechanisms. J. Virol. 84, 12646–12657 (2010).
40. A. M. Segura, O. H. Frazier, L. M. Buja, Fibrosis and heart failure. Heart Fail. Rev. 19, 173–185 (2014).
41. M. Maanja et al., Diffuse myocardial fibrosis reduces electrocardiographic voltage measures of left ventricular hypertrophy independent of left ventricular mass. J. Am. Heart Assoc. 6, e003795 (2017).
42. A. Pichlmair et al., RIG-I-mediated antiviral responses to single-stranded RNA bearing 5′-phosphates. Science 314, 997–1001 (2006).
43. F. Ma et al., Macrophage-stimulated cardiac fibroblast production of IL-6 is essential for TGF β/Smad activation and cardiac fibrosis induced by angiotensin II. PLoS One 7, e35144 (2012).
44. Z. R. Estabragh, M. A. Mamas, The cardiovascular manifestations of influenza: A systematic review. Int. J. Cardiol. 167, 2397–2403 (2013).
45. S. A. Sellers, R. S. Hagan, F. G. Hayden, W. A. Fischer, 2nd, The hidden burden of influenza: A review of the extra-pulmonary complications of influenza infection. Influenza Other Respir. Viruses 11, 372–393 (2017).
46. W. Witzleb, H. Witzleb, J. Mehlhorn, M. Sprössig, P. Wutzler, Demonstration of influenza virus A in human heart by semiquantitative virus assay and immunofluorescence. Acta Virol. 20, 168 (1976).
47. A. M. Cioc, G. J. Nuovo, Histologic and in situ viral findings in the myocardium in cases of sudden, unexpected death. Mod. Pathol. 15, 914–922 (2002).
48. C. G. Ray, T. B. Icenogle, L. L. Minnich, J. G. Copeland, T. M. Grogan, The use of intravenous ribavirin to treat influenza virus-associated acute myocarditis. J. Infect. Dis. 159, 829–836 (1989).
49. N. E. Bowles et al., Detection of viruses in myocardial tissues by polymerase chain reaction: Evidence of adenovirus as a common cause of myocarditis in children and adults. J. Am. Coll. Cardiol. 42, 466–472 (2003).
50. L. M. Wakim, N. Gupta, J. D. Mintern, J. A. Villadangos, Enhanced survival of lung tissue-resident memory CD8+ T cells during infection with influenza virus due to selective expression of IFITM3. Nat. Immunol. 14, 238–245 (2013).